Multi-ion Frequency Reference Using Dynamical Decoupling

Lennart Pelzer[1,*] Kai Dietze,[1,2] Víctor José Martínez-Lahuerta,[3,2] Ludwig Krinner,[1,2] Johannes Kramer,[1,2]
Fabian Dawel,[1,2] Nicolas C. H. Spethmann,[1] Klemens Hammerer,[3] and Piet O. Schmidt[1,2,†]

[1]*Physikalisch-Technische Bundesanstalt*, Bundesallee 100, 38116 Braunschweig, Germany
[2]*Institut für Quantenoptik, Leibniz Universität Hannover*, Welfengarten 1, 30167 Hannover, Germany
[3]*Institut für Theoretische Physik, Leibniz Universität Hannover*, Appelstraße 2, 30167 Hannover, Germany

We present the experimental realization of a continuous dynamical decoupling scheme which suppresses leading frequency shifts in a multi-ion frequency reference based on ^{40}Ca$^+$. By near-resonant magnetic coupling of the ^{2}S$_{1/2}$ and ^{2}D$_{5/2}$ Zeeman sublevels using radio-frequency dressing fields, engineered transitions with reduced sensitivity to magnetic-field fluctuations are obtained. A second stage detuned dressing field reduces the influence of amplitude noise in the first stage driving fields and decreases 2nd-rank tensor shifts, such as the electric quadrupole shift. Suppression of the quadratic dependence of the quadrupole shift to $3(2)$ mHz/μm^2 and coherence times of $290(20)$ ms on the optical transition are demonstrated even within a laboratory environment with significant magnetic field noise. Besides removing inhomogeneous line shifts in multi-ion clocks, the demonstrated dynamical decoupling technique may find applications in quantum computing and simulation with trapped ions by a tailored design of decoherence-free subspaces.

Decoherence and dephasing of quantum systems through interaction with the environment pose a major challenge for quantum sensors, quantum computers, and quantum simulators [1]. In particular, magnetic and electric fields can cause significant shifts that induce decoherence and dephasing due to their spectral noise properties and inhomogeneity across the quantum system. In optical clocks based on trapped ions, electric field gradients of the trapping potential couple to the electric quadrupole moment of the clock states causing a quadrupole shift (QPS) [2]. Several mitigation strategies have been developed to overcome these limitations. Technological solutions in the form of active stabilization and passive shielding have been demonstrated for magnetic fields in a variety of quantum systems [3–20]. However, most of these technical measures increase size and complexity of a setup, or cannot be eliminated by shielding, such as the QPS. In atomic clocks, mitigation strategies based on atomic properties include choosing magnetic field insensitive Zeeman levels, or averaging over several directions or Zeeman components, which at the same time eliminates the QPS [2,21–26]. However, many of these strategies fail for multi-ion clocks [27–31], since the shifts are inhomogeneous across the ion crystal, resulting in an effective broadening of the observed clock transition. A solution is provided by dynamical decoupling (DD), a technique that dates back to Hahn spin echoes in nuclear magnetic resonance spectroscopy [32].

Since then it has been further developed using pulsed [33,34] and continuous schemes [27,34–44], and employed experimentally in various systems to eliminate noise sources in quantum simulations [45], quantum computing [46–57], quantum memories [58–68], and quantum sensing [69–74]. In the context of precision spectroscopy and optical clocks, DD is implemented, e.g., by changing the magnetic field within a Ramsey sequence [75] or through precisely timed radio-frequency (rf) pulses that populate different Zeeman states to cancel undesired shifts within each individual interrogation. The latter has been demonstrated for QPS and magnetic field shift in ^{88}Sr$^+$ [76] and ^{176}Lu$^+$ [77], as well as employed to eliminate magnetic field shifts in a precision measurement of local Lorentz violation [78,79]. These pulsed schemes suppress noise sources with timescales slower than pulse intervals.

Here, we demonstrate the suppression of linear Zeeman shifts as well as the QPS on an optical transition in a trapped ^{40}Ca$^+$ frequency reference using a cascaded continuous dynamical decoupling (CDD) scheme with up to five ions. In contrast to similar pulsed schemes [76,77], here the levels are continuously coupling with rf fields to engineer an ensemble of robust artificial transitions by choosing adequate driving parameters [27,80]. This suppresses

inhomogeneous shifts across the ion crystal and mitigates noise up to half the Fourier frequencies corresponding to the rf Rabi frequency coupling of the Zeeman states. These artificial transitions can be treated similar to bare transitions, so, e.g., Rabi and Ramsey spectroscopy sequences as well as entangling operations are possible [80].

In the following we briefly summarize the CDD techniques employed here [27,80] and which are shown schematically in Fig. 1. The Zeeman manifolds of ground $^2S_{1/2}$ and excited $^2D_{5/2}$ levels are energetically split by a static external magnetic field with magnitude B_0 in the z direction

$$H_0 = \sum_{i=S,D} g_i \mu_B B_0 J_z^i = \sum_{i=S,D} \omega_0^i J_z^i. \qquad (1)$$

Here, the gyromagnetic factor g_i and spin operator z component J_z^i for each ensemble $i \in [S_{\frac{1}{2}}, D_{\frac{5}{2}}]$ as well as the Bohr magneton μ_B are used. These so-called bare atomic levels are coupled by near-resonant rf fields of the form

$$H_{rf} = \sum_{i=S,D} g_i \Omega_1^i \cos(\omega_1^i t) J_x^i - g_i \Omega_2^i \sin(\omega_1^i t) \cos(\omega_2^i t) J_x^i. \quad (2)$$

The first drive [first line in Eq. (2)] with frequency $\omega_1^i = \omega_0^i - \Delta_1^i$ and amplitude Ω_1^i produces a ladder of dressed states with frequency splitting

$$\bar{\omega}_0^i = \sqrt{(g_i \Omega_1^i/2)^2 + (\Delta_1^i)^2}. \qquad (3)$$

The second stage drive [2nd line in Eq. (2)] with frequency $\omega_2^i = \bar{\omega}_0^i - \Delta_2^i$ and amplitude Ω_2^i couples the first stage dressed states analogously to the first drive if the hierarchy of coupling frequencies $\omega_2^i \ll \omega_1^i$ is fulfilled. Here, collinear alignment of all rf drives is assumed for simplicity. For a detailed derivation of the general geometry we refer the reader to [80]. The two-stage design serves two purposes. First, temporal or spatial drive strength variations $\delta\Omega_1^i(\vec{r}, t)$ are mitigated, since assuming a constant fractional variation results in smaller absolute frequency shifts. Second, the additional drive adds control parameters to suppress Zeeman and 2nd-rank tensor shifts simultaneously as will be shown below. The so-called mixing angle $\cos(\theta_j^i) = \Delta_j^i/\bar{\omega}_j^i$ with $j \in [1, 2]$ and $i \in [S_{\frac{1}{2}}, D_{\frac{5}{2}}]$ determines the suppression of these shifts for each stage and manifold. In a doubly dressed basis, the response of the system to sufficiently slow magnetic field variations $\delta B(\vec{r}, t)$ can be described by

$$V_{\delta B} = \sum_{i=S,D} \cos(\theta_1^i) \cos(\theta_2^i) g_i \mu_B \delta B(\vec{r}, t) J_z^i \qquad (4)$$

and the quadrupole shift of the excited level by [80]

$$V_Q = (1 - 3\cos^2(\theta_1^D))(1 - 3\cos^2(\theta_2^D))$$
$$\times \Theta \frac{3}{8} \frac{\partial E_z}{\partial z} (J^D(J^D + 1) - 3(J_z^D)^2), \qquad (5)$$

using the spin of the D-level J^D. The magnitude of the shift depends on the quadrupole moment Θ and the electric field
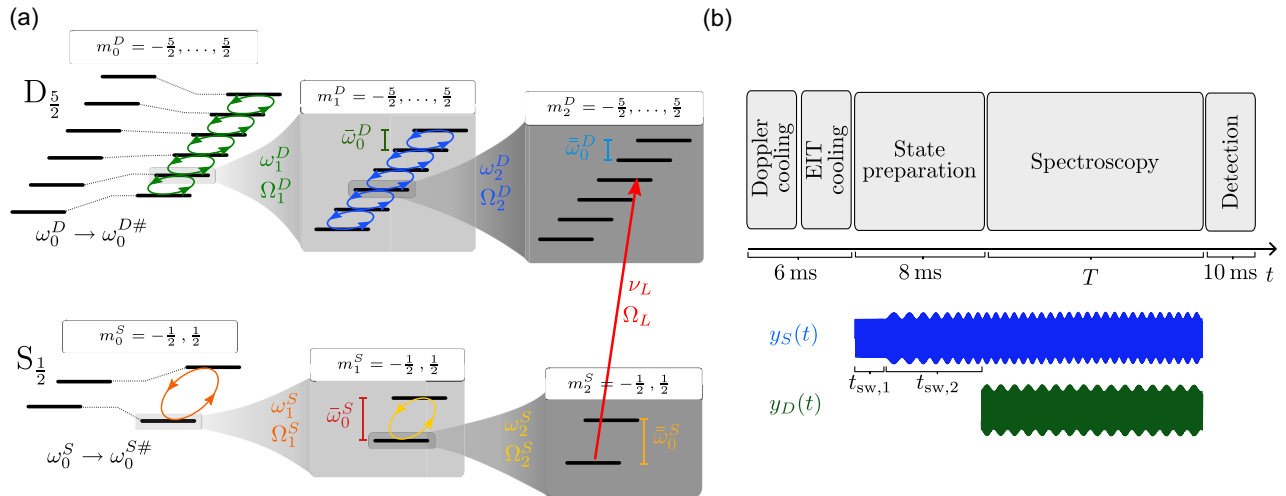

FIG. 1. (a) Continuous dynamical decoupling scheme. Near resonant rf coupling with driving frequency ω_j^i and strength Ω_j^i results in an ensemble of $2(J_j^i + 1)$ dressed states with spacing $\bar{\omega}_j^i$ and numbering m_j^i, where $j = 1, 2$ marks the 1st or 2nd layer of dressing and $i = S, D$ the Zeeman manifold. Here, the quantum numbers $J_1^S = 1/2 = J_2^S$ and $J_1^D = 5/2 = J_2^D$ match these of the spin of the underlying bare atomic states. Cross-coupling and Bloch-Siegert shifts result in a shift of the bare states' transition frequency $\omega_0^j \rightarrow \omega_0^{j\#}$. The doubly dressed transitions are probed with 729 nm light at frequency ν_L and coupling strength Ω_L. Adapted from [81] (b) Sketch of the spectroscopy sequence with typical durations. The lower part shows a sketch of the employed CDD waveforms with signal amplitudes y_i. Two successive frequency sweeps with durations $t_{sw,i}$ transfer the population adiabatically from the $^2S_{1/2}$ via the first dressed to the doubly dressed target state.

gradient $\partial E/\partial z$ [2], which is given by the joint potential of the trap and neighboring ions. It is worth noting that the suppression of both shifts is independent for both stages. This allows, e.g., suppression of the Zeeman shift using a resonant drive with $\theta_1^S = \theta_2^S = \theta_1^D = 0$ for all drives except the 2nd-stage D-level drive. QPS suppression can be attained using the so-called magic mixing angle on this last drive with $\cos^2(\theta_2^D) = \frac{1}{3}$ at the expense of a reduced Zeeman shift suppression. The achievable degree of suppression depends on the deviation of the angles θ_j^i from their ideal values. The detunings Δ_j^i are affected by magnetic field fluctuations acting on the bare atomic states, the QPS of the D states, frequency shifts from off-resonant cross coupling of the S drive on the D level and vice versa, as well as the correction of counterrotating terms in the rotating wave approximation (Bloch-Siegert shift) [27,80]. Since θ_j^i depends inversely proportional on Ω_j^i, the scheme becomes more robust against fluctuations in magnitude and noise frequency of these shifts for higher coupling strength at the expense of larger frequency shifts caused by amplitude noise of the rf drives, assuming a fixed fractional stability. The parameter set for optimum suppression is thus a trade-off between detuning fluctuations and driving strength, requiring a detailed knowledge of the noise properties of both.

In the setup presented here, the magnetic field noise causes line broadening on the order of $\nu_{\delta B} \lesssim 1$ kHz with a timescale on the order of milliseconds given by the mains supply and its harmonics. In contrast, the QPS is near static with an inhomogeneous shift of $\nu_{QPS} \lesssim 100$ Hz for typical trapping potentials. These characteristic timescales are slow compared to the inverse Rabi frequencies of the first (<25 µs) and second drive (<300 µs), respectively (compare [82]). A further discussion of the hierarchy of different timescales including the laser-ion coupling can be found in [80]. Assuming a realistic mixing angle mismatch of $\delta\theta = 1\%$, a Zeeman shift suppression on the order of $\cos(\theta_1^i)\cos(\theta_2^i) \approx 10^{-4}$ [compare Eq. (4)] for a doubly resonant drive and $(1 - 3\cos^2(\theta_2^D)) \approx 3 \times 10^{-2}$ QPS suppression [Eq. (5)] can be expected for small deviations. The additional inaccuracy of the scheme arises from a combination of the uncertainty in the coupling strength of all four drives Ω_j^i, and the uncertainty in the magnetic field, which affects the drive frequency detunings Δ_j^i. The frequency shift compared to the bare transition is a linear combination of the combined frequency splitting from each drive [Eq. (3)]. In the limit of negligible detuning error, the additional systematic uncertainty is directly proportional to the coupling strength uncertainty.

The majority of the experimental setup is described in detail elsewhere [81,83], therefore only key components are summarized here. $^{40}Ca^+$ ions are confined in a segmented Paul trap [84] with low excess micromotion even for axially extended crystals [28,83] as well as low motional heating due to on-chip filtering and a low noise

voltage supply [85]. All lasers needed for cooling, detection, and state preparation are locked to a wave meter [86]. The interrogation laser for the $^2S_{1/2} \leftrightarrow{}^2D_{5/2}$ transition at 729 nm is based on an amplified extended cavity diode laser [87], which is first prestabilized to a 10 cm cavity resulting in a fractional linewidth of 170(4) Hz. Further reduction of the laser linewidth is established by transfer locking [88,89] to a highly stable reference cavity [90] via a fiber-based frequency comb. An independent measurement revealed an upper limit for the fractional frequency instability of the $^{40}Ca^+$ clock laser against the reference laser of $\sigma_y < 2 \times 10^{-15}$ for $\tau > 1$ s. The reference laser reaches typically an instability of 5×10^{-17} for up to 10 s and a drift of 50 µHzs^{-1}. Therefore, the employed laser is not limiting for the following measurements.

A single aspheric lens is used for collecting fluorescence light of the ions. It is focused simultaneously onto a photomultiplier tube (PMT) and a scientific complementary metal-oxide-semiconductor (sCMOS) camera using a beam splitter. The PMT allows for discrimination of bright and dark states within 100 µs detection time [83]. Using the camera, spatially resolved detection of single ion excitation in a linear ion crystal is possible at the cost of a longer detection time of 10 ms, primarily attributable to the camera's readout process.

Three pairs of orthogonal magnetic field coils generate a static offset field of 357 µT along the axial trap direction resulting in 10 MHz splitting of the $^2S_{1/2}$ levels. The axial magnetic field component is actively stabilized against slow drifts using a fluxgate sensor and feedback to the current of the coils. Mains power synchronous magnetic field noise limits the linewidth of the $^2S_{1/2} \leftrightarrow{}^2D_{5/2}$ clock transition typically to $\Delta\nu \approx 100$ Hz. In addition, on timescales of ten seconds fluctuations on the order of $|\Delta B_0| \approx 5$ nT are observed.

Resonant magnetic field coils are employed for the CDD to shape and enhance the generated coupling waveforms. These rf coils consist of two separate, temperature-controlled LCR circuits with tunable capacitors to match the resonance frequency of the Zeeman ensembles [82].

The CDD sequence begins with the preparation of the target state in the dressed S levels. This is achieved through an adiabatic ramp from the bare ground state to the dressed level by applying a tailored waveform to the S coils via an arbitrary voltage generator [82]. A continuous transition without phase jumps from the preparation to the final second-stage waveform is crucial to maximize the contrast. The D-level waveform can be switched on instantaneously, since the D state is not populated and the cross-driving effect of the D-level drive onto the population in the S level is negligible. Spectroscopy within the CDD spectrum with the $^2S_{1/2}$ to $^2D_{5/2}$ laser at 729 nm is performed after the applied rf drives have reached their steady-state values. As long as the optical coupling is weak compared to the

rf coupling $\Omega_L \ll \Omega_i$ the fast dynamics of the manifold averages out and the artificial transitions can be treated analogously to a natural $^{40}Ca^+$ clock transition. In the following the $|S_{1/2}, m_0^S = -\frac{1}{2}, m_1^S = \frac{1}{2}, m_2^S = \frac{1}{2}\rangle \leftrightarrow |D_{5/2}, m_0^D = -\frac{3}{2}, m_1^D = \frac{1}{2}, m_2^D = \frac{1}{2}\rangle$ transition (compare Fig. 1) is probed with the clock laser directed along the static magnetic field and trap axis. With the employed parameters [82], a magnetic field shift sensitivity of $-1.2(1) \times 10^{-4}$ Hz/nT^2 was determined in a separate measurement. This represents an almost four orders of magnitude improvement over the sensitivity of the bare states of 5.6 Hz nT^{-1} for typical field variations of 5 nT and is comparable to clock species with magnetic-field sensitivity only from nuclear spin, such as $^{27}Al^+$ and $^{115}In^+$ [91,92]. Therefore, a coherence time of 0.29(2) s can be observed on one of the artificial transitions (see Fig. 2). The optical coupling strength of each transition between dressed states depends on the selection rules of the underlying Zeeman transition as well as on mixing angles and quantum numbers of the dressed state [80].

In order to demonstrate the capabilities of this scheme we probe the line shifts of a linear five-ion crystal. Such a system is a stringent test for a multi-ion frequency reference. In Fig. 3 the comparison of inhomogeneous line shifts along the crystal for two different CDD-parameter sets is shown. The frequencies of the first stage rf fields are held close to the respective splitting of the Zeeman states $\Delta_1^S = 0 = \Delta_1^D$. The detuning of the 2nd D-level stage is set for the two cases $\Delta_2^D = 0$ and $\Delta_2^D = 1/\sqrt{8}g_D\Omega_2^D$, corresponding to the resonant and magic mixing angle, respectively. In the first case only Zeeman shifts are suppressed, the second also suppresses 2nd-rank tensor shifts at the cost of reduced Zeeman shift suppression. A relative QPS suppression factor of 12 was measured between resonant and magic detuned parameter set

[Figs. 3(b) and 3(c)], measured by the quadratic fitting parameter of 3(2) mHz/μm². Simultaneously, the linear term increases by a factor of 3, caused by lower suppression of the magnetic field inhomogeneity. In a third setting, the CDD parameters are fine-tuned by an offset of the static B field such that the imperfections in residual inhomogeneous static and dynamic B field partially compensate, which allows suppression of the overall frequency spread across the 20 μm long crystal to 1.8(7) Hz [Fig. 3(d)]. Further optimization by variation of all CDD parameters is likely to improve the results. However, technical measures for enhanced homogeneity and stability of the fields will loosen the requirements to find the optimal parameters. The slow temporal variations of the leading frequency shifts, namely, residual amplitude fluctuations of the CDD drive and of the magnetic field, are measured to be on the level of $|\delta\Omega_i/\Omega_i| < 6 \times 10^{-5}$ and $|\delta B_0/B_0| < 2 \times 10^{-5}$, respectively. These were determined by observing the splitting of bare and first-stage dressed states over several 100 s.

The frequency instability of the doubly dressed transition of a five-ion crystal is displayed in Fig. 4. With the chosen
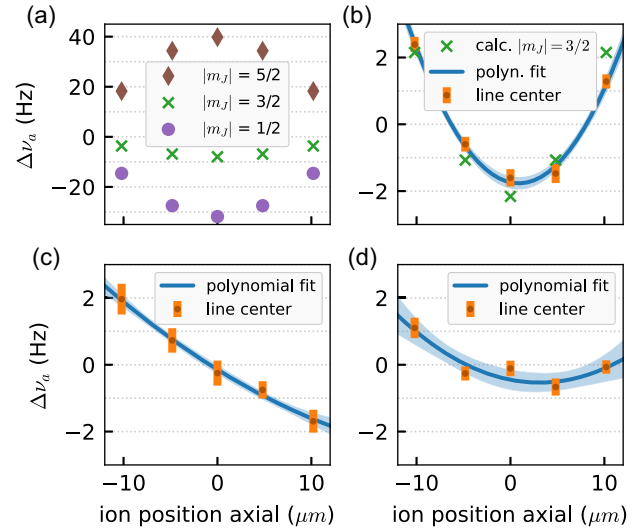
FIG. 3. Comparison of the relative frequency shifts of the artificial clock transition along a linear five-ion crystal for different CDD parameters. The individual line centers are obtained from a scan of the clock laser with fitting of individual peaks using ion-resolved camera data. (a) Calculated QPS for five-ion crystal for bare Zeeman levels. Ion positions are simulated in a pure harmonic potential with given trapping frequencies to extract field gradients at the ion positions. (b) Doubly resonant parameter set ($\Delta_j^i = 0 \ \forall \ i, j$). Tensorial shifts are of equal size compared to the calculated $|m_J| = \frac{3}{2}$ bare level shift (green crosses). (c) Magic angle detuned second stage D-level CDD drive. The visible linear dependency arises from magnetic field inhomogeneity in combination with lower Zeeman shift suppression compared to (b). (d) Same CDD drive as for (c), but optimized offset B field for field inhomogeneity compensation.
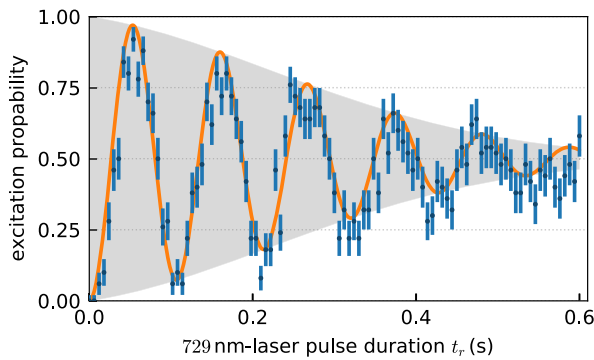

FIG. 2. 729 nm pulse time scan of a doubly dressed artificial transition. The strong Zeeman shift suppression with resonant driving parameters allows a long coherence time. The data are in good agreement with a combined Gaussian and exponential decay model $P_e(t_r) = \frac{1}{2}(1 - \cos(2\pi\Omega_L t_r)e^{-t_r/\Gamma}e^{-t_r^2/(2\gamma^2)})$ with given natural decay $\Gamma = 1.168$ [93] and $\gamma = 0.29(2)$ s. The Gaussian decay shape indicates long noise correlation times with respect to the duration of an individual data point [94].
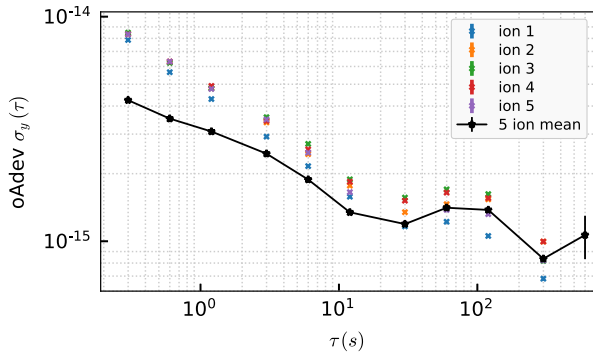
FIG. 4. Overlapping Allan deviation of the relative frequency stability of a linear five-ion crystal. Two-point sampling Rabi interrogation with 100 ms interrogation time and duty cycle of 33% was used. The excitation probability of the individual ions was measured using an sCMOS camera. The sensitivity to small dynamic or offset magnetic field variations depends on the absolute field value. Therefore, inhomogeneous fields cause stability differences for the individual ions.

parameters, a gain in statistical uncertainty due to increased ion number is given up to 10 s averaging time. Strong residual magnetic field noise components at 0.01 Hz compromise the stability. The Zeeman shift sensitivity depends on the absolute field at the position of each ion, therefore the stability varies for the individual ions, particularly visible on ion 1. However, the short-term instability of $3 \times 10^{-15}/\sqrt{\tau}$ is comparable to $^{40}Ca^+$ clocks with multilayer magnetic shielding [95]. Increasing the interrogation duty cycle from $T/T_c = 33\%$ to $\approx 90\%$ will be possible with a faster experimental control system together with faster camera detection and readout.

In conclusion, we have demonstrated the suppression of linear Zeeman shifts and QPS on an artificial clock transition through CDD. The presented CDD scheme is especially useful for transitions with strong electronic linear Zeeman shift. This lifts the need for elaborate shielding and reduces the statistical uncertainty in clocks by enabling longer interrogation times. By reducing magnetic field noise and drive field inhomogeneity, as well as implementing faster camera detection, a larger number of ions would enable this frequency reference to be used as a flywheel in composite, multispecies clocks [96–99]. To the best of our knowledge, this is the first time a 2-stage CDD scheme has been successfully implemented, which might prove useful for other quantum sensors or qubit systems that are limited by magnetic field sensitivity.

[*] Contact author: lennart.pelzer@ptb.de
[†] Contact author: piet.schmidt@quantummetrology.de

[1] A. Acín, I. Bloch, H. Buhrman, T. Calarco, C. Eichler, J. Eisert, Daniel Esteve, N. Gisin, S. J. Glaser, F. Jelezko, S. Kuhr, M. Lewenstein, M. F. Riedel, P. O. Schmidt, R. Thew, A. Wallraff, I. Walmsley, and F. K. Wilhelm, New J. Phys. **20**, 080201 (2018).

[2] W. M. Itano, J. Res. NIST **105**, 829 (2000).

[3] B. Merkel, K. Thirumalai, J. E. Tarlton, V. M. Schäfer, C. J. Ballance, T. P. Harty, and D. M. Lucas, Rev. Sci. Instrum. **90**, 044702 (2019).

[4] M. Zeng, Z. Ma, R. Hu, B. Zhang, Y. Hao, H. Zhang, Y. Huang, H. Guan, and K. Gao, Chin. Phys. B **32**, 110704 (2023).

[5] M. Borkowski, L. Reichsöllner, P. Thekkeppatt, V. Barbé, T. van Roon, K. van Druten, and F. Schreck, Rev. Sci. Instrum. **94**, 073202 (2023).

[6] Z.-X. Duan, W.-T. Wu, Y.-T. Lin, and S.-J. Yang, Rev. Sci. Instrum. **93**, 123201 (2022).

[7] I. Altarev *et al.*, Rev. Sci. Instrum. **85**, 075106 (2014).

[8] E. A. Dijck, C. Warnecke, M. Wehrheim, R. B. Henninger, J. Eff, K. Georgiou, A. Graf, S. Kokh, L. P. Kozhiparambil Sajith, C. Mayo, V. M. Schäfer, C. Volk, P. O. Schmidt, T. Pfeifer, and J. R. Crespo López-Urrutia, Rev. Sci. Instrum. **94**, 083203 (2023).

[9] Y.-H. Ji, L. Zhou, S.-T. Yan, C. He, C. Zhou, S. Barthwal, F. Yang, W.-T. Duan, W.-D. Zhang, R.-D. Xu, Q. Wang, D.-X. Li, J.-H. Gao, X. Chen, J. Wang, and M.-S. Zhan, Rev. Sci. Instrum. **92**, 083201 (2021).

[10] T. Leopold, S. A. King, P. Micke, A. Bautista-Salvador, J. C. Heip, C. Ospelkaus, J. R. Crespo López-Urrutia, and P. O. Schmidt, Rev. Sci. Instrum. **90**, 073201 (2019).

[11] A. Farolfi, D. Trypogeorgos, G. Colzi, E. Fava, G. Lamporesi, and G. Ferrari, Rev. Sci. Instrum. **90**, 115114 (2019).

[12] J. A. Devlin, E. Wursten, J. A. Harrington, T. Higuchi, P. E. Blessing, M. J. Borchert, S. Erlewein, J. J. Hansen, J. Morgner, M. A. Bohman, A. H. Mooser, C. Smorra, M. Wiesinger, K. Blaum, Y. Matsuda, C. Ospelkaus, W. Quint, J. Walz, Y. Yamazaki, and S. Ulmer, Phys. Rev. Appl. **12**, 044012 (2019).

[13] E. Wodey, D. Tell, E. M. Rasel, D. Schlippert, R. Baur, U. Kissling, B. Kölliker, M. Lorenz, M. Marrer, U. Schläpfer, M. Widmer, C. Ufrecht, S. Stuiber, and P. Fierlinger, Rev. Sci. Instrum. **91**, 035117 (2020).

[14] J. Vovrosh, G. Voulazeris, P. G. Petrov, J. Zou, Y. Gaber, L. Benn, D. Woolger, M. M. Attallah, V. Boyer, K. Bongs, and M. Holynski, Sci. Rep. **8,** 2023 (2018).

[15] M. F. Brandl, M. W. van Mourik, L. Postler, A. Nolf, K. Lakhmanskiy, R. R. Paiva, S. Möller, N. Daniilidis, H. Häffner, V. Kaushal, T. Ruster, C. Warschburger, H. Kaufmann, U. G. Poschinger, F. Schmidt-Kaler, P. Schindler, T. Monz, and R. Blatt, Rev. Sci. Instrum. **87,** 113103 (2016).

[16] I. Altarev, M. Bales, D. H. Beck, T. Chupp, K. Fierlinger, P. Fierlinger, F. Kuchler, T. Lins, M. G. Marino, B. Niessen, G. Petzoldt, U. Schläpfer, A. Schnabel, J. T. Singh, R. Stoepler, S. Stuiber, M. Sturm, B. Taubenheim, and J. Voigt, J. Appl. Phys. **117,** 183903 (2015).

[17] S.-K. Lee and M. V. Romalis, J. Appl. Phys. **103,** 084904 (2008).

[18] A. Mager, IEEE Trans. Magn. **6,** 67 (1970).

[19] R. J. Hanson and F. M. Pipkin, Rev. Sci. Instrum. **36,** 179 (1965).

[20] T. Ruster, C. T. Schmiegelow, H. Kaufmann, C. Warschburger, F. Schmidt-Kaler, and U. G. Poschinger, Appl. Phys. B **122,** 254 (2016).

[21] P. Dubé, A. A. Madej, J. E. Bernard, L. Marmet, J.-S. Boulanger, and S. Cundy, Phys. Rev. Lett. **95,** 033001 (2005).

[22] H. S. Margolis, G. P. Barwood, G. Huang, H. A. Klein, S. N. Lea, K. Szymaniec, and P. Gill, Science **306,** 1355 (2004).

[23] M. Chwalla, J. Benhelm, K. Kim, G. Kirchmair, T. Monz, M. Riebe, P. Schindler, A. Villar, W. Hänsel, C. F. Roos, R. Blatt, M. Abgrall, G. Santarelli, G. Rovera, and Ph. Laurent, Phys. Rev. Lett. **102,** 023002 (2009).

[24] P. Dubé, A. A. Madej, Z. Zhou, and J. E. Bernard, Phys. Rev. A **87,** 023806 (2013).

[25] W. H. Oskay, W. M. Itano, and J. C. Bergquist, Phys. Rev. Lett. **94,** 163001 (2005).

[26] T. Schneider, E. Peik, and Chr. Tamm, Phys. Rev. Lett. **94,** 230801 (2005).

[27] N. Aharon, N. Spethmann, I. D. Leroux, P. O. Schmidt, and A. Retzker, New J. Phys. **21,** 083040 (2019).

[28] J. Keller, T. Burgermeister, D. Kalincev, A. Didier, A. P. Kulosa, T. Nordmann, J. Kiethe, and T. E. Mehlstäubler, Phys. Rev. A **99,** 013405 (2019).

[29] K. Arnold, E. Hajiyev, E. Paez, C. H. Lee, M. D. Barrett, and J. Bollinger, Phys. Rev. A **92,** 032108 (2015).

[30] N. Herschbach, K. Pyka, J. Keller, and T. E. Mehlstäubler, Appl. Phys. B **107,** 891 (2012).

[31] C. Champenois, M. Marciante, J. Pedregosa-Gutierrez, M. Houssin, and M. Knoop, Phys. Rev. A **81,** 043410 (2010).

[32] E. L. Hahn, Phys. Rev. **80,** 580 (1950).

[33] L. Viola, E. Knill, and S. Lloyd, Phys. Rev. Lett. **82,** 2417 (1999).

[34] C. H. Valahu, I. Apostolatos, S. Weidt, and W. K. Hensinger, J. Phys. B **55,** 204003 (2022).

[35] M. Cai and K. Xia, Phys. Rev. A **106,** 042434 (2022).

[36] İ. Yalçınkaya, B. Çakmak, G. Karpat, and F. F. Fanchini, Quantum Inf. Process. **18,** 156 (2019).

[37] I. Cohen, N. Aharon, and A. Retzker, Fortschr. Phys. **65,** 1600071 (2017).

[38] G. Mikelsons, I. Cohen, A. Retzker, and M. B. Plenio, New J. Phys. **17,** 053032 (2015).

[39] N. Aharon, M. Drewsen, and A. Retzker, Phys. Rev. Lett. **111,** 230507 (2013).

[40] A. Bermudez, P. O. Schmidt, M. B. Plenio, and A. Retzker, Phys. Rev. A **85,** 040302(R) (2012).

[41] J.-M. Cai, B. Naydenov, R. Pfeiffer, L. P. McGuinness, K. D. Jahnke, F. Jelezko, M. B. Plenio, and A. Retzker, New J. Phys. **14,** 113023 (2012).

[42] A. Z. Chaudhry and J. Gong, Phys. Rev. A **85,** 012315 (2012).

[43] P. Facchi, D. A. Lidar, and S. Pascazio, Phys. Rev. A **69,** 032314 (2004).

[44] L. Viola and S. Lloyd, Phys. Rev. A **58,** 2733 (1998).

[45] W. Morong, K. S. Collins, A. De, E. Stavropoulos, T. You, and C. Monroe, PRX Quantum **4,** 010334 (2023).

[46] P. Barthel, P. H. Huber, J. Casanova, I. Arrazola, D. Niroomand, T. Sriarunothai, M. B. Plenio, and C. Wunderlich, New J. Phys. **25,** 063023 (2023).

[47] A. D. Leu, M. F. Gely, M. A. Weber, M. C. Smith, D. P. Nadlinger, and D. M. Lucas, Phys. Rev. Lett. **131,** 120601 (2023).

[48] C. Fang, Y. Wang, S. Huang, K. R. Brown, and J. Kim, Phys. Rev. Lett. **129,** 240504 (2022).

[49] B. Pokharel, N. Anand, B. Fortman, and D. A. Lidar, Phys. Rev. Lett. **121,** 220502 (2018).

[50] A. Stark, N. Aharon, A. Huck, H. A. R. El-Ella, A. Retzker, F. Jelezko, and U. L. Andersen, Sci. Rep. **8,** 14807 (2018).

[51] J. Randall, S. Weidt, E. D. Standing, K. Lake, S. C. Webster, D. F. Murgia, T. Navickas, K. Roth, and W. K. Hensinger, Phys. Rev. A **91,** 012322 (2015).

[52] T. R. Tan, J. P. Gaebler, R. Bowler, Y. Lin, J. D. Jost, D. Leibfried, and D. J. Wineland, Phys. Rev. Lett. **110,** 263002 (2013).

[53] S. C. Webster, S. Weidt, K. Lake, J. J. McLoughlin, and W. K. Hensinger, Phys. Rev. Lett. **111,** 140501 (2013).

[54] A. M. Souza, G. A. Álvarez, and D. Suter, Phys. Rev. A **86,** 050301(R) (2012).

[55] A. Noguchi, S. Haze, K. Toyoda, and S. Urabe, Phys. Rev. Lett. **108,** 060503 (2012).

[56] X. Xu, Z. Wang, C. Duan, P. Huang, P. Wang, Y. Wang, N. Xu, X. Kong, F. Shi, X. Rong, and J. Du, Phys. Rev. Lett. **109,** 070502 (2012).

[57] I. V. Zalivako, A. S. Borisenko, I. A. Semerikov, A. Korolkov, P. L. Sidorov, K. Galstyan, N. V. Semenin, V. Smirnov, M. A. Aksenov, A. K. Fedorov, K. Y. Khabarova, and N. N. Kolachevsky, Front. Quantum Sci. Technol. **2,** 1228208 (2023).

[58] P. Wang, C.-Y. Luan, M. Qiao, M. Um, J. Zhang, Y. Wang, X. Yuan, M. Gu, J. Zhang, and K. Kim, Nat. Commun. **12,** 233 (2021).

[59] G. A. Sinuco-Leon, H. Mas, S. Pandey, G. Vasilakis, B. M. Garraway, and W. von Klitzing, Phys. Rev. A **104,** 033307 (2021).

[60] G. A. Sinuco-Leon, B. M. Garraway, H. Mas, S. Pandey, G. Vasilakis, V. Bolpasi, W. von Klitzing, B. Foxon, S. Jammi, K. Poulios, and T. Fernholz, Phys. Rev. A **100,** 053416 (2019).

[61] D. Trypogeorgos, A. Valdés-Curiel, N. Lundblad, and I. B. Spielman, Phys. Rev. A **97,** 013407 (2018).

[62] A. Laucht, R. Kalra, S. Simmons, J. P. Dehollain, J. T. Muhonen, F. A. Mohiyaddin, S. Freer, F. E. Hudson, K. M. Itoh, D. N. Jamieson, J. C. McCallum, A. S. Dzurak, and A. Morello, Nat. Nanotechnol. **12,** 61 (2017).

[63] J. Zhang, A. M. Souza, F. D. Brandao, and D. Suter, Phys. Rev. Lett. **112,** 050502 (2014).

[64] D. A. Golter, T. K. Baldwin, and H. Wang, Phys. Rev. Lett. **113,** 237601 (2014).

[65] G.-Q. Liu, H. C. Po, J. Du, R.-B. Liu, and X.-Y. Pan, Nat. Commun. **4,** 2254 (2013).

[66] M. J. Biercuk, H. Uys, A. P. VanDevender, N. Shiga, W. M. Itano, and J. J. Bollinger, Nature (London) **458,** 996 (2009).

[67] N. Timoney, I. Baumgart, M. Johanning, A. F. Varon, M. B. Plenio, A. Retzker, and Ch. Wunderlich, Nature (London) **476,** 185 (2011).

[68] G. de Lange, Z. H. Wang, D. Ristè, V. V. Dobrovitski, and R. Hanson, Science **330,** 60 (2010).

[69] M. Zhang, Y. Xie, J. Zhang, W. Wang, C. Wu, T. Chen, W. Wu, and P. Chen, Phys. Rev. Appl. **15,** 014033 (2021).

[70] I. Baumgart, J.-M. Cai, A. Retzker, M. B. Plenio, and Ch. Wunderlich, Phys. Rev. Lett. **116,** 240801 (2016).

[71] S. Kotler, N. Akerman, Y. Glickman, A. Keselman, and R. Ozeri, Nature (London) **473,** 61 (2011).

[72] L. T. Hall, C. D. Hill, J. H. Cole, and L. C. L. Hollenberg, Phys. Rev. B **82,** 045208 (2010).

[73] L. M. Pham, N. Bar-Gill, C. Belthangady, D. Le Sage, P. Cappellaro, M. D. Lukin, A. Yacoby, and R. L. Walsworth, Phys. Rev. B **86,** 045214 (2012).

[74] M. Bishof, X. Zhang, M. J. Martin, and J. Ye, Phys. Rev. Lett. **111,** 093604 (2013).

[75] R. Lange, N. Huntemann, C. Sanner, H. Shao, B. Lipphardt, Chr. Tamm, and E. Peik, Phys. Rev. Lett. **125,** 143201 (2020).

[76] R. Shaniv, N. Akerman, T. Manovitz, Y. Shapira, and R. Ozeri, Phys. Rev. Lett. **122,** 223204 (2019).

[77] R. Kaewuam, T. R. Tan, K. J. Arnold, S. R. Chanu, Z. Zhang, and M. D. Barrett, Phys. Rev. Lett. **124,** 083202 (2020).

[78] C.-H. Yeh, K. C. Grensemann, L. S. Dreissen, H. A. Fürst, and T. E. Mehlstäubler, New J. Phys. **25,** 093054 (2023).

[79] L. S. Dreissen, C.-H. Yeh, H. A. Fürst, K. C. Grensemann, and T. E. Mehlstäubler, Nat. Commun. **13,** 7314 (2022).

[80] V. J. Martínez-Lahuerta, L. Pelzer, K. Dietze, L. Krinner, P. O. Schmidt, and K. Hammerer, Quantum Sci. Technol. **9,** 015013 (2024).

[81] L. Pelzer, Robust artificial clock transition by continuous dynamical decoupling in multi-ion calcium crystals, Ph.D. thesis, Leibniz Unversität Hannover, 2023, 10.15488/13239.

[82] See Supplemental Material at http://link.aps.org/supplemental/10.1103/PhysRevLett.133.033203 for details on generating the radio-frequency waveforms used for continuous dynamical decoupling.

[83] S. Hannig, L. Pelzer, N. Scharnhorst, J. Kramer, M. Stepanova, Z. T. Xu, N. Spethmann, I. D. Leroux, T. E. Mehlstäubler, and P. O. Schmidt, Rev. Sci. Instrum. **90,** 053204 (2019).

[84] K. Pyka, N. Herschbach, J. Keller, and T. E. Mehlstäubler, Appl. Phys. B **114,** 231 (2014).

[85] N. Beev, J.-A. Fenske, S. Hannig, and P. O. Schmidt, Rev. Sci. Instrum. **88,** 054704 (2017).

[86] High Finesse WS U10.

[87] TA pro Toptica.

[88] J. Stenger, H. Schnatz, C. Tamm, and H. R. Telle, Phys. Rev. Lett. **88,** 073601 (2002).

[89] N. Scharnhorst, J. B. Wübbena, S. Hannig, K. Jakobsen, J. Kramer, I. D. Leroux, and P. O. Schmidt, Opt. Express **23,** 19771 (2015).

[90] D. G. Matei, T. Legero, S. Häfner, C. Grebing, R. Weyrich, W. Zhang, L. Sonderhouse, J. M. Robinson, J. Ye, F. Riehle, and U. Sterr, Phys. Rev. Lett. **118,** 263202 (2017).

[91] T. Rosenband, P. O. Schmidt, D. B. Hume, W. M. Itano, T. M. Fortier, J. E. Stalnaker, K. Kim, S. A. Diddams, J. C. J. Koelemeij, J. C. Bergquist, and D. J. Wineland, Phys. Rev. Lett. **98,** 220801 (2007).

[92] E. Peik, G. Hollemann, and H. Walther, Phys. Rev. A **49,** 402 (1994).

[93] A. Kreuter, C. Becher, G. P. T. Lancaster, A. B. Mundt, C. Russo, H. Häffner, C. Roos, W. Hänsel, F. Schmidt-Kaler, R. Blatt, and M. S. Safronova, Phys. Rev. A **71,** 032504 (2005).

[94] T. Monz, Quantum information processing beyond ten ion-qubits, Ph.D. thesis, University of Innsbruck, 2011.

[95] Y. Huang, B. Zhang, M. Zeng, H. Zhang, Y. Hao, Z. Chen, M. Wang, H. Guan, and K. Gao, preprint 10.21203/rs.3.rs-120082/v1 (2021).

[96] D. B. Hume and D. R. Leibrandt, Phys. Rev. A **93,** 032138 (2016).

[97] S. Dörscher, A. Al-Masoudi, M. Bober, R. Schwarz, R. Hobson, U. Sterr, and C. Lisdat, Commun. Phys. **3,** 1 (2020).

[98] T. Rosenband and D. R. Leibrandt, arXiv:1303.6357.

[99] J. Borregaard and A. S. Sørensen, Phys. Rev. Lett. **111,** 090802 (2013).